AD-A067 593 CAMBRIDGE UNIV (ENGLAND) DEPT OF ENGINEERING F/G 11/6
FRACTURE-MECHANISMS IN TWO AUSTENITIC AND ONE FERRITIC STEEL.(U)
DEC 78 M F ASHBY, R J FIELDS, T WEERASOORIYA DA-ERO-76-G-060

UNCLASSIFIED NL

| OF |
AD
AD67593

END
DATE
FILMED
6 -79
DDC

FRACTURE-MECHANISMS IN TWO AUSTENITIC AND ONE FERRITIC STEEL.

M.F. Ashby[+], R.J. Fields[*], and T. Weerasooriya[+]

DECEMBER 1978

+Cambridge University
Engineering Department
Trumpington Street
Cambridge CB2 1PZ

*National Bureau of Standards
Washington, D.C., U.S.A.

Abstract

The mechanisms of fracture of round tensile specimens of two austenitic stainless steels (types 304 and 316) and one ferritic steel ($2\frac{1}{4}$ Cr-1 % Mo) have been studied. These new observations have been combined with published information to construct two types of fracture-mechanism diagram which show the regions of dominance of each mechanism, and summarise the fracture observations between absolute zero and melting point. These diagrams may help in distinguishing between creep-brittle and creep-ductile batches of steel, and in the rational extrapolation of creep-rupture data.

UNCLASSIFIED

SECURITY CLASSIFICATION OF THIS PAGE *(When Data Entered)*

R&D 2324

REPORT DOCUMENTATION PAGE

READ INSTRUCTIONS BEFORE COMPLETING FORM

1. REPORT NUMBER	2. GOVT ACCESSION NO.
3. RECIPIENT'S CATALOG NUMBER	
4. TITLE (and Subtitle) FRACTURE-MECHANISMS IN TWO AUSTENITIC AND ONE FERRITIC STEEL	5. TYPE OF REPORT & PERIOD COVERED FINAL TECHNICAL REPORT, AUG 76 — DEC 78
	6. PERFORMING ORG. REPORT NUMBER
7. AUTHOR(s) M. F. ASHBY, R. J. FIELDS, T. WEERASOORIYA	8. CONTRACT OR GRANT NUMBER(s) DAERO-76-G-060
9. PERFORMING ORGANIZATION NAME AND ADDRESS ENGINEERING DEPARTMENT, UNIVERSITY OF CAMBRIDGE, CAMBRIDGE U.K.	10. PROGRAM ELEMENT, PROJECT, TASK AREA & WORK UNIT NUMBERS 6.11.02A-1T161102BH57-04-00-595
11. CONTROLLING OFFICE NAME AND ADDRESS U.S. ARMY R&S GRP (EUR), BOX 65, FPO NEW YORK 09510	12. REPORT DATE DECEMBER 1978
	13. NUMBER OF PAGES 25
14. MONITORING AGENCY NAME & ADDRESS *(if different from Controlling Office)*	15. SECURITY CLASS. *(of this report)* UNCLASSIFIED
	15a. DECLASSIFICATION/DOWNGRADING SCHEDULE

16. DISTRIBUTION STATEMENT *(of this Report)*

APPROVED FOR PUBLIC RELEASE

DISTRIBUTION UNLIMITED

17. DISTRIBUTION STATEMENT *(of the abstract entered in Block 20, if different from Report)*

18. SUPPLEMENTARY NOTES

19. KEY WORDS *(Continue on reverse side if necessary and identify by block number)*

(U) FRACTURE MAPS
(U) FRACTURE MECHANISMS
(U) CREEP
(U) DUCTILE FRACTURE
(U) BRITTLE FRACTURE

20. ABSTRACT *(Continue on reverse side if necessary and identify by block number)*

"SEE OVER"

DD FORM 1 JAN 73 1473 EDITION OF 1 NOV 65 IS OBSOLETE

UNCLASSIFIED 400 081

SECURITY CLASSIFICATION OF THIS PAGE (When Data Entered)

LB

20. ABSTRACT:

The mechanisms of fracture of round tensile specimens of two austenitic stainless steels (types 304 and 316) and one ferritic steel (2¼ Cr-1 % Mo) have been studied. These new observations have been combined with published information to construct two types of fracture-mechanism diagram which show the regions of dominance of each mechanism, and summarise the fracture observations between absolute zero and melting point. These diagrams may help in distinguishing between creep-brittle and creep-ductile batches of steel, and in the rational extrapolation of creep-rupture data.

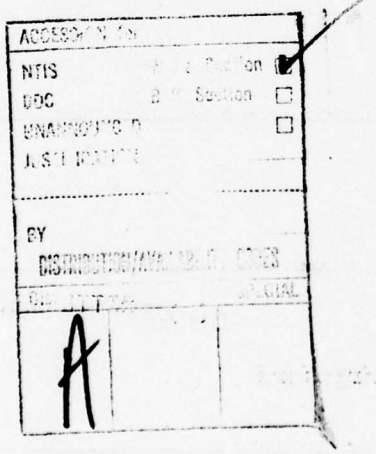

1. INTRODUCTION

In this paper, we attempt to catalog the mechanisms of fracture of the two austenitic and one ferritic steels, and to determine the regime of stress, temperature and time-to-fracture over which each is dominant. It extends and builds on the work of Wray (1969) who observed three modes of fracture in 316, and who presented his results as a diagram showing the regime of dominance of intergranular failure in strain-rate/temperature space.

1.1 Type 304 and 316 Stainless Steels

The 18-8 austenitic stainless steels have properties which are exploited commercially over a wide range of temperature: from the cryogenic (4.2 K) to the creep (650 ^{o}C) regimes. Over this range they exhibit at least three distinct modes of failure: ductile fracture, transgranular creep fracture, and intergranular creep fracture. At still higher temperatures (> 900 ^{o}C) a fourth mode - rupture - appears. Embrittling heat-treatments or corrosive environments can introduce still other modes of failure.

Type 304 is typical of the 18-8 series. It is a solid solution of about 18% chromium and 8% nickel in iron, with sufficient carbon that $Cr_{23}C_6$ and other carbides may appear during service at high temperatures. Type 316 is a more creep resistant alloy, containing (in addition to the chromium and nickel) about 2½% of molybdenum, a powerful carbide-former; again, carbides appear during service, and may be precipitated in a controlled way by ageing.

There is some variation in the mechanical properties of different heats of both these steels. Compositional differences are one reason for this. Table 1 shows that the permitted range of compositions for these alloys is a wide one. In addition, the properties of the 18-8 series depend on their thermal and mechanical history: in the case of 316, for instance,

homogenizing and quenching followed by deformation and aging gives higher strengths, both at room temperature, and (for short times) at high temperatures (Garafalo et al, 1961 (a)). Finally, there is the problem of the sensitization in these steels: if they are cooled slowly through the range 800 to 400 °C, they become susceptible to corrosion and oxidation at grain boundaries, and to premature intergranular failure. For these reasons, we have focussed primarily on data for steels which had been homogenized at about 1200K and quenched in oil or water, although some effects of other treatments will be discussed.

But even when the heat treatment is standardised, there remain certain unexplained variations in the fracture behaviour - particularly the creep-ductility - of these alloys. It is known that precipitation continues throughout even the longest creep tests of 316, and probably of 304. Typically, carbides of the $M_{23}C_6$ type appear first, and while they slowly coarsen, a grain-boundary sigma-phase (an intermetallic of the FeCr type) and a chi-phase (approximating $Fe_{36}C_{12}M_{10}$) appear (Weiss and Stickler, 1972). Strain influences the topology and kinetics of the precipitation, and so, too, do the concentrations of carbon and boron in the alloy (Donati, 1977; Lai, 1977; Marshall, 1977), thereby influencing the mechanical properties in a way which is not yet fully understood.

1.2 *The 2¼Cr-1Mo Ferritic Steel*

The low-alloy ferritic steels are widely used for turbine casings and pipe work. That described here is a 2¼%Cr 1%Mo steel, used for evaporator and superheater tubes in conventional and nuclear power-plant. The initial heat treatment, (homogenisation at 960 °C, followed by furnace cooling at less than 100 °C/hour) results in a fine precipitate of Mo_2C, which transforms to $M_{23}C_6$ and M_6C (or possibly M_4C) with time (Leitnaker, 1975). This dispersion may coarsen further during use at high temperature, depleting the matrix of chromium and molybdenum, with consequent loss of high-temperature strength. The ferritic steels exhibit all the fracture mechanisms listed earlier,

and, in addition, they cleave. (See also the study of pure iron by Fields and Ashby 1978).

2. NEW OBSERVATIONS AND DATA

2.1 Experimental Method

We tested round-section tensile specimens of the three steels. The austenitic samples were BSC type 304 and 316, machined from bar stock, homogenised at 1323K for one hour and quenched in water. The ferritic samples were homogenised at 1220K and furnace cooled. Their compositions are given in Table 1. At low temperatures (< 400 ^{o}C) the specimens were pulled to fracture in air at a constant strain-rate, in a time of about 10^2 sec. Above this temperature, the specimens were tested in a conventional creep machine, in vacuum, under constant load. We recorded the nominal tensile stress (σ_n), the temperature (T), the strain ($\varepsilon_f = \ln \ell_f/\ell_o$) and time ($t_f$) to fracture, and the final reduction in area ($\varepsilon_a = \ln A_o/A_f$), where ℓ_o and A_o are the initial length and cross-section, and ℓ_f and A_f their value at fracture. The fracture surfaces and sections through the fractured specimens were examined by optical and scanning microscopy, to identify the mode of failure. In plotting the results, temperatures were normalised by dividing by the melting point of pure iron (1810K), and stresses were normalised by dividing them by Young's modulus E, at the temperature of the test. For this purpose, we used Blackburn's (1972) data for E for 304 and 315, which, if linearised, is described by

$$E(T) = 2.16 \times 10^5 \, (1 - 4.7 \times 10^{-4}(T-300)) \text{ MN/m}^2$$

That for the ferritic steel was described by a polynomial fitted to the curve given by Fields and Ashby (1978), and calculated from the single-crystal constants of Dever (1972) and Lord and Beshers (1964) for pure iron:

$$E(T) = 1.96 \times 10^5 \, (1 - 2.1 \times 10^{-4} \, (T-300) - 1.7 \times 10^{-7} \, (T-300)^2 - 3.2 \times 10^{-10}(T-300)^3) \text{ MN/m}^2$$

Here T is the absolute temperature.

2.2 *Observations of Fracture Mechanisms for the Stainless Steels*

The observations will be illustrated by micrographs for 316. Type 304 behaved in an almost identical way.

From 77K to about 650K, the steels failed by *low-temperature ductile fracture*. Fig. 1a shows the nature of the fracture surface of 316 at room temperature, and typifies this sort of fracture. There is considerable necking, and a fibrous or dimpled fracture surface. Sectioning and etching shows that holes nucleate at angular particles which we believe, because of their shape and reaction to various standard etches, to be chromium-rich spinels ($MgAl_2O_4$). The holes then elongate parallel to the tensile axis, finally linking to form the cup of the cup-and-cone fracture. The fracture surface shows coarse dimples corresponding to the spinel inclusions overlaid by finer dimples caused by holes which may have nucleated on carbides.

Fast creep tests in the range of temperature between 650 and 1200K results in a transgranular creep fracture which, in many ways, resembles that observed at room temperature (Fig. 1b). There are differences, however. Necking is still pronounced, but the extension to fracture is reduced. The fracture surface is dimpled, but the dimple spacing is larger the higher the temperature; at 900K it corresponds roughly to the spacing of spinel inclusions. The holes still elongate along the tensile axis, but the extent of elongation is less at the higher temperature suggesting that they link more readily.

Both the extension, ε_f, and the area reduction, ε_a, at fracture are larger at lower temperatures. But if the extensions are subtracted from the area reductions, it is found that the post-necking strain ($\varepsilon_a - \varepsilon_f$) is almost constant, and roughly equal to 0.25. The specimens differ in the amount of homogeneous strain they undergo before necking; and this in turn reflects the way in which the work-hardening characteristics and the strain-rate sensitivity of the material change with temperature. At low temperatures (< 650K)

the material work hardens strongly and can be thought of as a rate-independent plastic solid; at higher temperatures (> 650K) it work-hardens less strongly, but is rate-dependent, and properly thought of as a creeping solid. For this reason, we distinguish *transgranular creep fracture* from *low-temperature ductile fracture*, even though the processes of hole nucleation, growth and linkage in both have much in common.

At lower stresses, in the temperature range from 650 to 1200K, both stainless steels failed by *intergranular creep fracture*. Fig. 1c shows typical results, obtained at 873K. The samples show little elongation and even less necking; surface cracking and boundary cavitation lead to a failure which, in this instance, is almost 100% intergranular. The steels we examined were "creep-brittle"; the transition to the low-ductility intergranular mode occurred at failure times of only a few hours. Data and maps are presented both for this and for a "creep ductile" batch of 316 in Section 3.

Above 1200K both steels fail by *rupture*; necking to zero cross-section. This may result from the resolution of the carbides and the other inclusions, thereby removing the nuclei for cavity formation. There is evidence of dynamic recrystallisation in this regime: the grains in the severely necked section of the specimen were found, after failure, to be almost equiaxed.

2.3 *Observation of Fracture Mechanisms for the Ferritic Steel*

A similar study was made of the 2¼Cr-1Mo steel (Weerasooriya, 1978). Between 77K and 200K the steel failed by *cleavage*. Fracture began at machining marks which act as nuclei for cleavage cracks, and propagated by cleavage of grains, alternating with brittle intergranular separation. In this mode of failure, reduction in area at the fracture is almost zero.

Between 200K and 400K the fracture was ductile, closely resembling that of Fig. 1a. At higher temperatures the number of cavities decreased and their size increased with increasing temperature and (at 675 ^{o}C) with decreasing stress.

In none of our tests (which covered temperatures up to 675 ^{o}C and times up to 10^7 secs) did we observe grain boundary cavitation or wedge cracking;

all creep failures were transgranular. Intergranular fracture, and the transitional mixed mode of fracture, have, however, been observed at fracture times exceeding 10^7 secs (Needham, 1971; Smith, 1971; B.S.C.C., 1971). These results have been used in positioning the field boundaries on Figs 5.

The fracture mechanisms observed in this steel parallel those observed in pure iron, (Fields and Ashby, 1978) though the extent and position of the fields has been much changed by the alloying. In particular, the transgranular creep fracture field is much larger, and lies at a higher stress level, for the steel, making it a creep-ductile material.

3. FRACTURE-MECHANISM MAPS FOR THE THREE STEELS

3.1 Construction of the Maps

Maps which summarise the fracture behaviour of the three steels are shown as Figs 2, 3, 4 and 5. The procedure used to construct such maps is described in detail elsewhere, (Ashby, 1978; Fields and Ashby, 1978). Those shown here combine fractographic information from published work with our own observations.

The first sort of map is shown in Figs 2a, 3a, 4a and 5a. The axes are *normalised tensile stress*, σ_n/E, and *homologous temperature*, T/T_M, and they span the range of conditions for which the material is solid. Data from the sources indicated on the figures are plotted as open symbols if the fracture was transgranular, and full symbols if the fracture was intergranular; they are labelled with the $\log_{10}$ of the time-to-fracture. The map is divided into fields which contain all observations of a given mode of fracture. The field boundaries (heavy lines) indicate our estimate of the mid-point of the transition from one mechanism to another. The shading on either side indicates the width of the transition - within the shaded region a mixed mode of fracture is observed. Superimposed on the fields are contours of constant time-to-fracture. They were arrived at by interpolation between the data points.

An alternative way of presenting the data is shown in Figs 2b, 3b, 4b and 5b. Here the axes are those of the conventional stress-rupture plot: log (tensile stress) and log (failure time). Data obtained at one temperature is connected by a line and labelled with the temperature. The field boundaries from the first sort of fracture map have been cross-plotted onto these diagrams, dividing them into fields in which (as before) a given mechanism of fracture is dominant. Data obtained at a single temperature is linked by a line, and shading shows the transition from one mechanism to the next.

We have truncated all the maps at a stress which would lead to a strain rate of about 10^6/sec. Above this stress level, fracture becomes a dynamic problem, limited by the velocity of elastic or plastic waves within the material. Although the detailed failure mechanisms here may resemble those observed in slower tests, extrapolation of the field boundaries into this regime is not justified.

3.2 *Maps for Low Boron, Homogenised and Quenched, 304 and 316*

Maps for standard 304 and 316 are shown in Figs 2 and 3. The positions of the field boundaries are based on published work by Smith et al (1950), Dulis et al (1953), Simmons et al (1965), Sanderson et al (1969), and our own observations, all of which appear to be mutually consistent. The maps show the fields of dominance of each of the four fracture modes, and regions of shading which indicate the approximate width of the transition zone between them.

Both materials are "creep-brittle", they exhibit a transition to a low-ductility, intergranular fracture mode at failure times of only a few hours, and a very small field of transgranular creep fracture. In this they contrast with the maps shown as Figs 4 and 5, which describe "creep-ductile" materials.

The plots emphasise that a change in slope of the creep rupture plot often reflects a change in fracture mechanism. But one must remember that, in an alloy like 316 which derives part of its strength from carbide and intermetallic precipitates, changes in microstructure may overlay changes in fracture

mechanism. The map for 316 (Fig. 3b) shows evidence of this: at about 10^7 seconds, the plots show unexplained changes in slope, through which we have drawn a heavy broken line. We have not yet been able to examine specimens which have failed at these long times, and do not know whether it is the shape and distribution of the intergranular cracks which has changed (as they do in pure iron, Fields and Ashby, 1978) or whether a change in precipitate distribution, caused by long ageing under stress, has caused a change in the kinetics of intergranular cracking.

We have identified the field boundary separating ductile transgranular fracture from transgranular creep fracture with the U.T.S. of the steel in normal tensile tests ($t_f \sim 10^2$ s). If the initial stress is greater than this, the material can be regarded as a (rate-independent) plastic solid which fails more or less instantaneously, in a ductile manner. If the initial stress is less than this, failure is not instantaneous, but requires the accumulation of creep strain. Though crude, this criterion is straight-forward and uses existing data; that of Sanderson et al (1969), Simmons et al (1965) and our own observations.

The boundary separating intergranular from transgranular creep fracture on the two figures was positioned to be consistent with the fractographic observations of Smith et al (1950). Positioned in this way, the boundary coincides more or less exactly with a change in slope of the stress-rupture plots presented by Smith et al (1950), and is consistent with our own observations and with those of Garofalo et al (1961a) who report that fracture was intergranular in all their tests.

Above about 1200K (0.65 T_M), intergranular fracture in both 304 and 316 is suppressed; the steels neck extensively and fail by plastic rupture (Nadai and Manjoine, 1941; Wray, 1969). This behaviour is common among commercially pure f.c.c. metals and alloys (Gandhi et al, 1978), where it appears to be associated with dynamic recrystallisation. In the stainless steels this, in turn, may be triggered by the solution of certain of the

carbide precipitates: $M_{23}C_6$ carbides in 18-8 stainless steels are known to dissolve somehwere between 800 and 900 °C (Aborn and Bain, 1930). As the carbides (and possibly the oxides) dissolve, the number of nucleating sites decreases, and boundaries migrate away from cavities which formed on them, leaving them harmlessly within the new grain.

3.3 *Maps for High-Boron 316*

Intergranular cavitation in stainless steels appears to be made more difficult by the presence of boron, particularly if the carbon content is low. The steels described in the previous section were not deliberately innoculated with boron, and showed cavitation after only 10 to 100 hours. Some boron-containing stainless steels do not show cavitation even after many thousand hours under load at high temperatures. It appears, too, that cold or warm working, followed by ageing, can decrease the creep rate and increase the life, though it makes the steel more susceptible to recrystallisation or accelerated grain growth, even at relatively low temepratures ($\sim$ 500 °C) if the fracture life is several years or more. Grain boundary movement may suppress the growth of intergranular cavities and so favour a transgranular fracture mode.

A limited amount of fractographic and creep data is available for high boron (> 50 ppm) 316 steels, heat treated at 1050 °C and air cooled. It is summarised in Figs 4. Although the times to fracture are not much changed by the doping and the altered heat treatment, the extent of the transgranular creep-fracture field has increased enormously.

3.4 *Maps for 2¼ Cr-1Mo Steel*

The mechanical properties of 2¼Cr-1Mo steel depend on its previous thermal and mechanical treatment. For this reason, it is necessary to consider bars, pipe and plates separately. The maps shown as Fig. 5 apply strictly only to material from pipe in the annealed state, though we would expect plate and bar to be broadly similar.

The maps show the areas of dominance of five fracture mechanisms, separated by shaded, transitional regions of mixed fracture mode. The parts of the maps referring to the ferritic state of the steel are based on the work of Needman (1971) and on our own observations. In certain places the position of a field boundary has been inferred from changes in ductility, though this has been done only if it was consistent with fractographic observations. The data of Smith (1971) and B.S.C.C. (1971), for example, show a drastic reduction in both ε_f and ε_a in long term creep tests, implying that a regime of fully intergranular fracture exists.

The fracture behaviour of the steel above the $\alpha - \gamma$ transition has been assumed to be the same as that of nominally pure austenite. Data for this material, and a map summarising it, has been presented by Fields and Ashby (1978).

4. CONCLUSIONS AND APPLICATIONS

4.1 Fracture Mechanism Maps for Steels

Observations of the tensile fracture of a steel from OK to the melting point can be summarised as a *fracture mechanism map*. The map shows the region of stress, time and temperatures over which a given mechanism of fracture is dominant, and is based on experimental creep data and fractographic studies of the steel. We have found that, although data was drawn from many different sources, there is little ambiguity in defining the boundaries of these regions or fields for steels of closely similar composition and heat treatment. The resulting map gives a broad and self-consistent picture of the way the material behaves. Maps are presented for type 304 and type 316 stainless steel, and for a 2¼%Cr-1%Mo ferritic steel.

Pure metals and solid solutions are well described by a single map (Gandhi, Ashby and Taplin, 1978). But the steels studied here derive a large part of their strength from a dispersion, and the kinetics of its precipitation and coarsening depend on previous thermal and mechanical history, and on

trace levels of impurities. We have found for instance, that the maps for low-boron, homogenised and quenched 316 differ from those for a high boron, homogenised and air-cooled 316 in the relative size of the fields of transgranular and of intergranular creep fracture. And, whereas in pure metals fracture is caused by a purely mechanical instability, in these steels (and other similar alloys) the mechanical instability may reflect a microstructural instability, like overageing, or the precipitation of a new phase which is brittle, or has poor coherence to the matrix.

4.2 *Extrapolation of Creep Data*

Within a field of the fracture map a single mechanism is dominant. Even though it may be influenced by microstructural changes, it seems likely that *within a field* a simple, empirical extrapolation procedure (as is presently used for the engineering extrapolation of creep data) should be satisfactory. But on crossing a field boundary the mechanism - and its underlying kinetics and stress-dependence - changes, and there is no justification for further extrapolation (even though it may sometimes appear to work in practice).

This presents a particular problem with the "creep-ductile" 316, and the 2¼%Cr-1%Mo pipe steel of Figs 4 and 5. Almost all the data for both steels lies in the transgranular creep fracture field - a field characterised by large elongation and reduction in area at fracture. Yet it appears certain that, at sufficiently long times, an intergranular mechanism, with low elongation and reduction in area, will appear - and limited experimental data supports this view. Figs 4 and 5 show that this switch of mechanism may well occur at times shorter than the design life of structures in which these steels are used, making extrapolation (particularly as it relates to creep ductility) particularly hazardous.

But the maps may be of help here. Figs 4b and 5b suggest a C-shaped field boundary between trans- and intergranular fracture. The shortest times at which the transition occurs are at the nose of the C. By choosing test conditions near this nose, it may be possible to determine, from tests which

are practical in the laboratory, where the transition takes place, and how much the ductility falls when it has done so.

References

Aborn, R.H. and Bain, E.C. (1930) Trans. Amer. Soc. Steel Treating 18, 837.

Ashby, M.F. (1978) to appear in Acta Met.

Blackburn, L.D., *The Generation of Isochronous Stress Strain Curves*, A.S.M.E. Winter Annual Meeting New York, Nov. 1972, Publisher A.S.M.E.

Bolton, C.J., Cordwell, J.E., Hooper, A.J., Marshall, P., Steeds, J. and Wickens, A. (1977) C.E.G.B. report RD/B/N3991, September, 1977.

B.S.C.C. (1971) High Temperature Data, The Iron and Steel Institute, p. 356-400.

B.S.C.C. (1972/1973) British Steel Corporation ISO/TC17/SC10/ETP-SG (Secretariat 104) 138-MT/QF/54/74, p. 11.

Dever, D.J. (1972) J. Appl. Phys 43, 3293.

Donati, R. (1977) EdF, Department "Etude des Matériaux", Les Renardieres, France, Private Communication.

Dulis, E.J., Smith, G.V. and Houston, E.G. (1953) Trans. A.S.M. 45, 42.

Fields, R.J. and Ashby, M.F. (1978) to appear in Acta Met.

Gandhi, C., Ashby, M.F. and Taplin, D.M.R. (1978) to be published.

Garofalo, F., Whitmore, R.W., Domis, W.F. and von Gemmingen, F. (1961 a) Trans. Metall. Soc. A.I.M.E., 221, 310.

Garofalo, F., von Gemmingen, F., Domis, W.F. (1961 b) Trans. A.S.M. 54, 430.

I.N.C.O. (1974) Datasheet *Materials for Cryogenic Service: Austenitic Stainless Steels: Engineering Properties*, International Nickel Ltd, London.

Johnson, R.F., May, M.J., Truman, R.J., and Mickleraith, J. (1966) Proc. Joint Conf. by British Iron and Steel Res. Ass. and Institute, p. 229.

Klueh, R.L. and Oakes, R.E. (1976) J. Eng. Mat. and Technology, 98, 361.

Lai, J. (1977) Private communication.

Leitnaker, J.M., Klueth, R.L. and Laing, W.R. (1975) Met. Trans. 6A, 1949.

Lord, A.E. and Beshers, D.N. (1964) J. Appl. Phys. 35, 2397.

Marshall, P. (1977) Private communication.

Nadai, A. and Manjoine, M.J. (1941) J. Appl. Mechanics 63, A-77.

Needham, N. (1971) Product Research, B.S.C. Report No. PROD/PS/5923/1/71/A.

Parr, J.G. and Hanson, A. (1965) *An Introduction to Stainless Steel*, A.S.M., Metals Park, Ohio.

Sanderson, G.P. and Llewellyn, D.J. (1969) J.I.S.I., 207, 1129.

Simmons, W.J. and van Echo, J.A. (1965) A.S.T.M. Data Series Publ. DS5-S1.

Smith, G.V. (1971) A.S.T.M. data series No. D.S. 652.

Smith, G.V., Dulis, E.J. and Houston, E.G. (1950) Trans. A.S.M. 42, 935.

Weiss, B. and Stickler, R. (1972) Met. Trans. 3, 851.

Wray, P.J. (1969) J. Appl. Phys. 40, 4018.

Weerasooriya, T. (1978) "Biaxial Fatigue Properties at 565 ^{o}C and Deformation Properties of 2$\frac{1}{4}$Cr-1Mo Steel" Ph.D. Thesis, Cambridge University.

ACKNOWLEDGEMENTS

This work was supported by the U.S. Army under Contract Number DAERO-7-G-060. One of us (T.W.) wish to acknowledge the support of the Commonwealth Scholarship Agency, U.K. We are most grateful to Dr. P.J. Wray, of the U.S. Steels Research Centre, for his advice and help in providing unpublished data.

Figure 1 - Three modes of fracture in a low boron, homogenised and quenched type 316 steel.

1 (a) Ductile fracture at room temperature (σ_n = 613 MN/m^2; T = 293K; ε_f = 0.52; A_f = 0.78; t_f = 2.7 × 10^2 s).

1 (b) Transgranular creep fracture at 600 ^{o}C (σ_n = 399 MN/m^2; T = 873K; ε_f = 0.29; A_f = 0.53; t_f = 6.1 × 10^3 s).

1 (c) Intergranular creep fracture at 600 ^{o}C (σ_n = 84 MN/m^2; T = 873K, ε_f = 0.11; A_f = 0.17; 1.3 × 10^6 s).

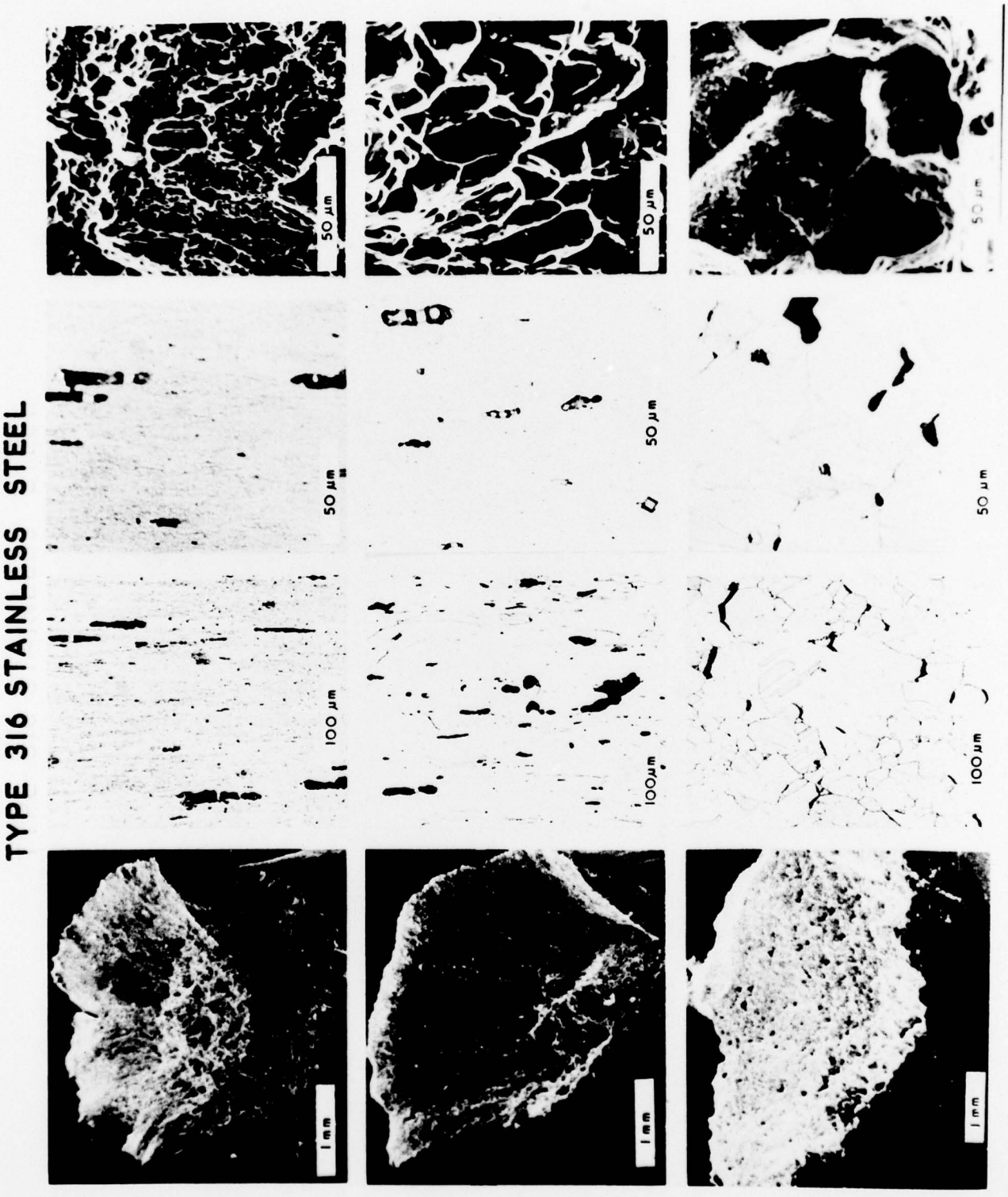
TYPE 316 STAINLESS STEEL
a
DUCTILE FRACTURE (20°C)
b
TRANSGRANULAR CREEP FRACTURE (500°C,399MN/m²)
c
INTERGRANULAR CREEP FRACTURE (600°C,84MN/m²)
1 mm
100 µm
50 µm

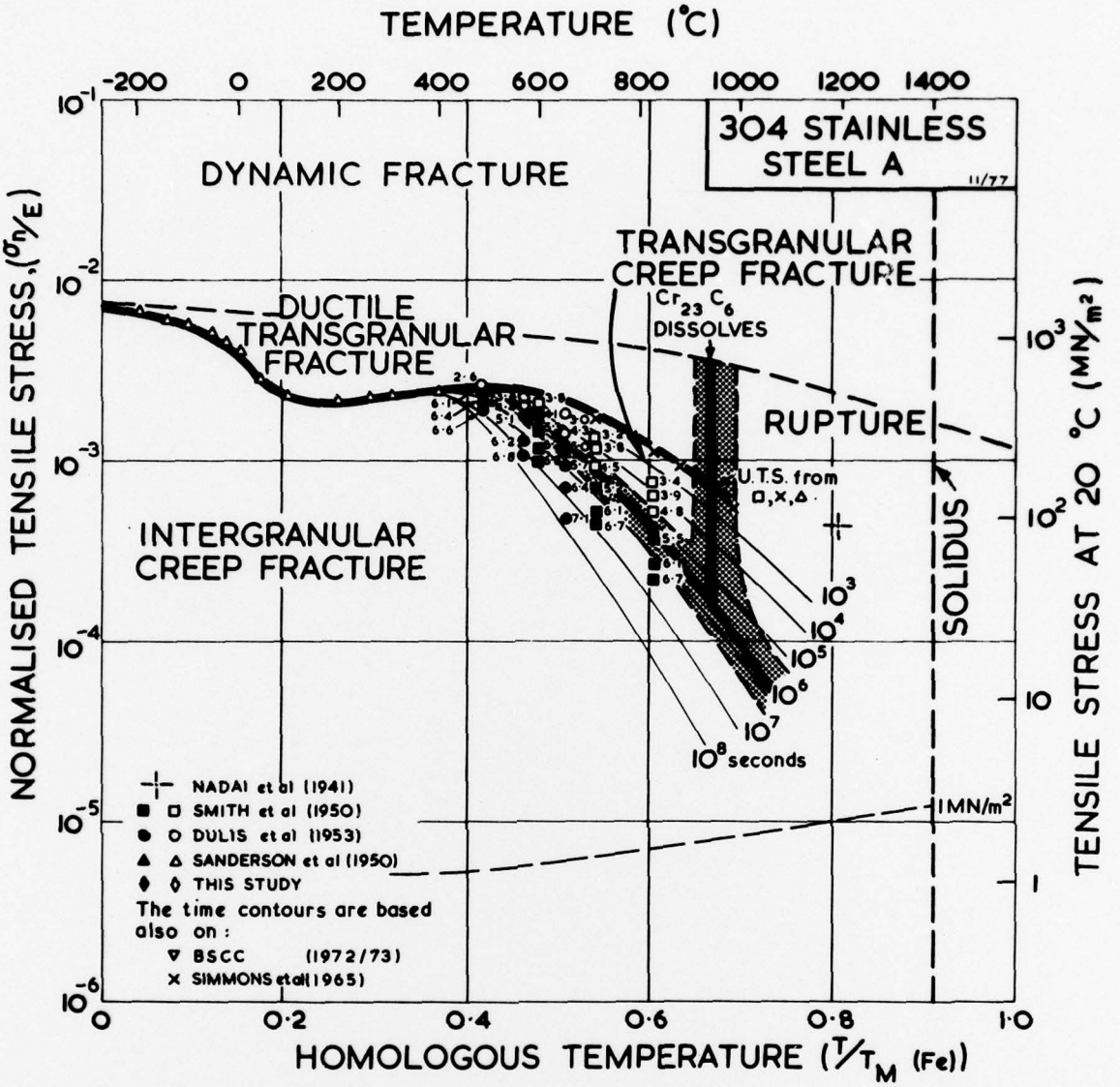

Figure 2

2 (a) A fracture map of the first type for low-boron, homogenised and quenched 304 stainless steel.

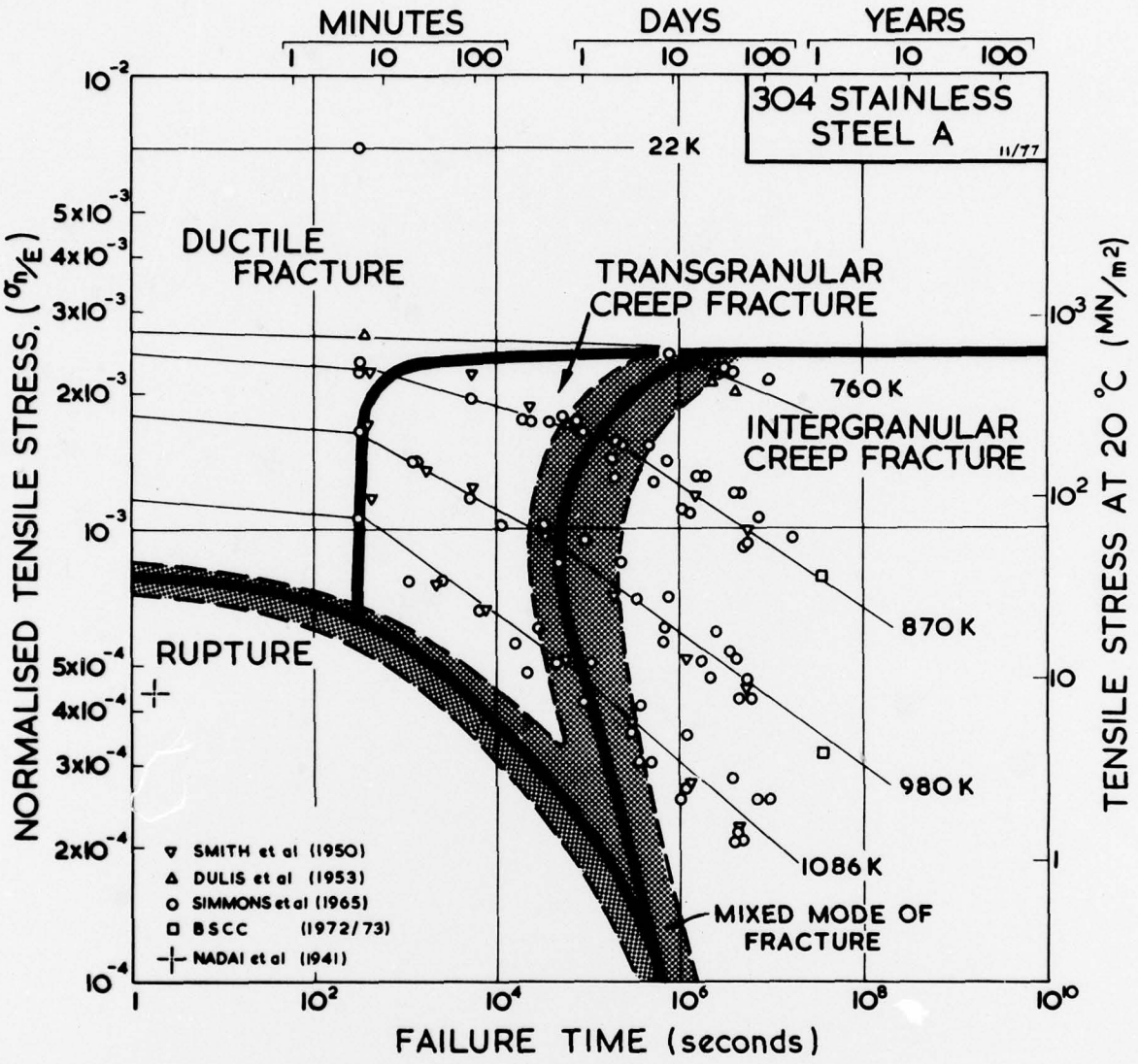

2 (b) A map of the second type for the same steel. The field boundaries have been cross-plotted from Fig. 2(a). Shading indicates a mixed, or transitional, mode of fracture.

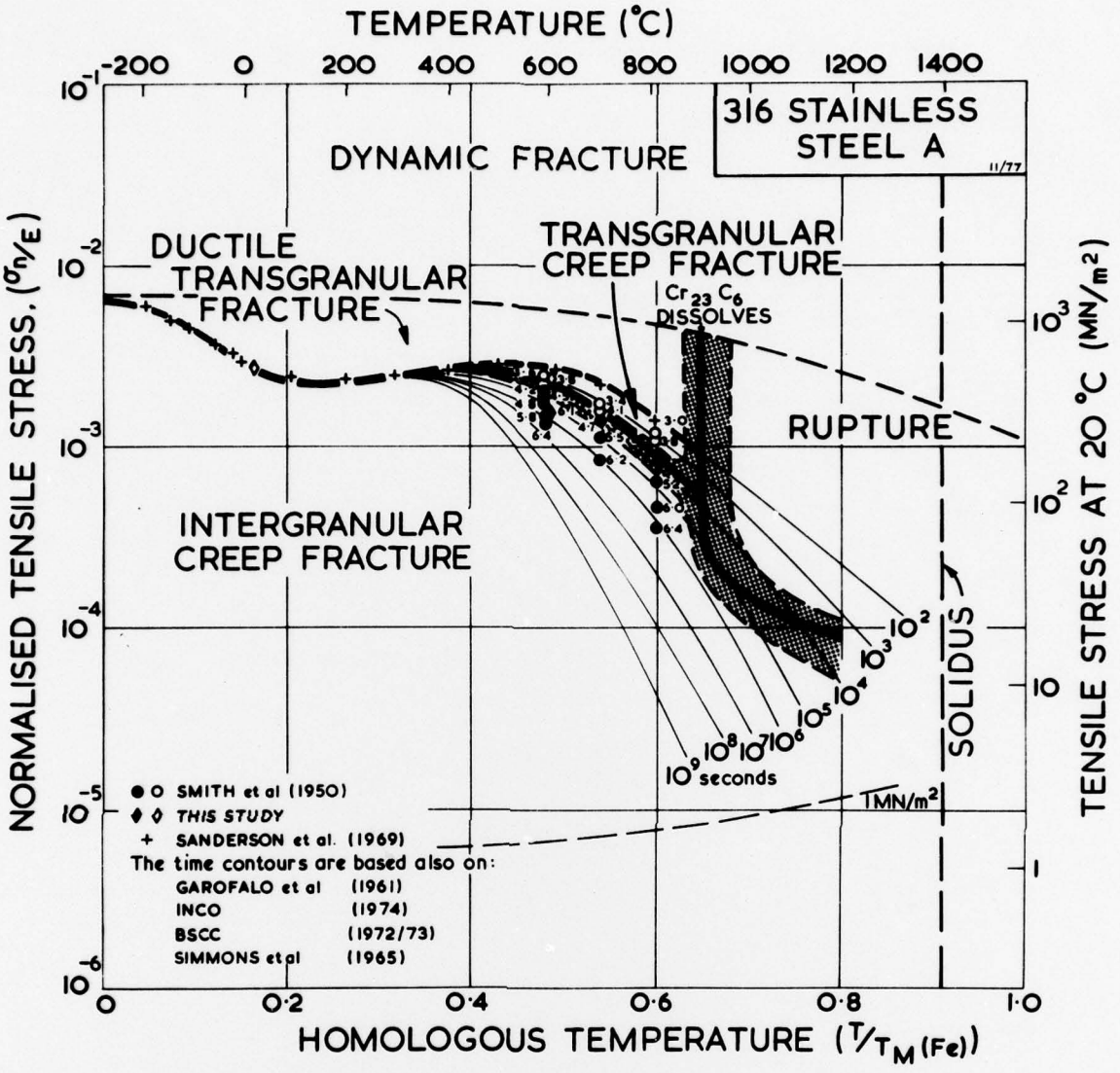

Figure 3

3 (a) A fracture map of the first type for low-boron, homogenised and quenched, 316 stainless steel.

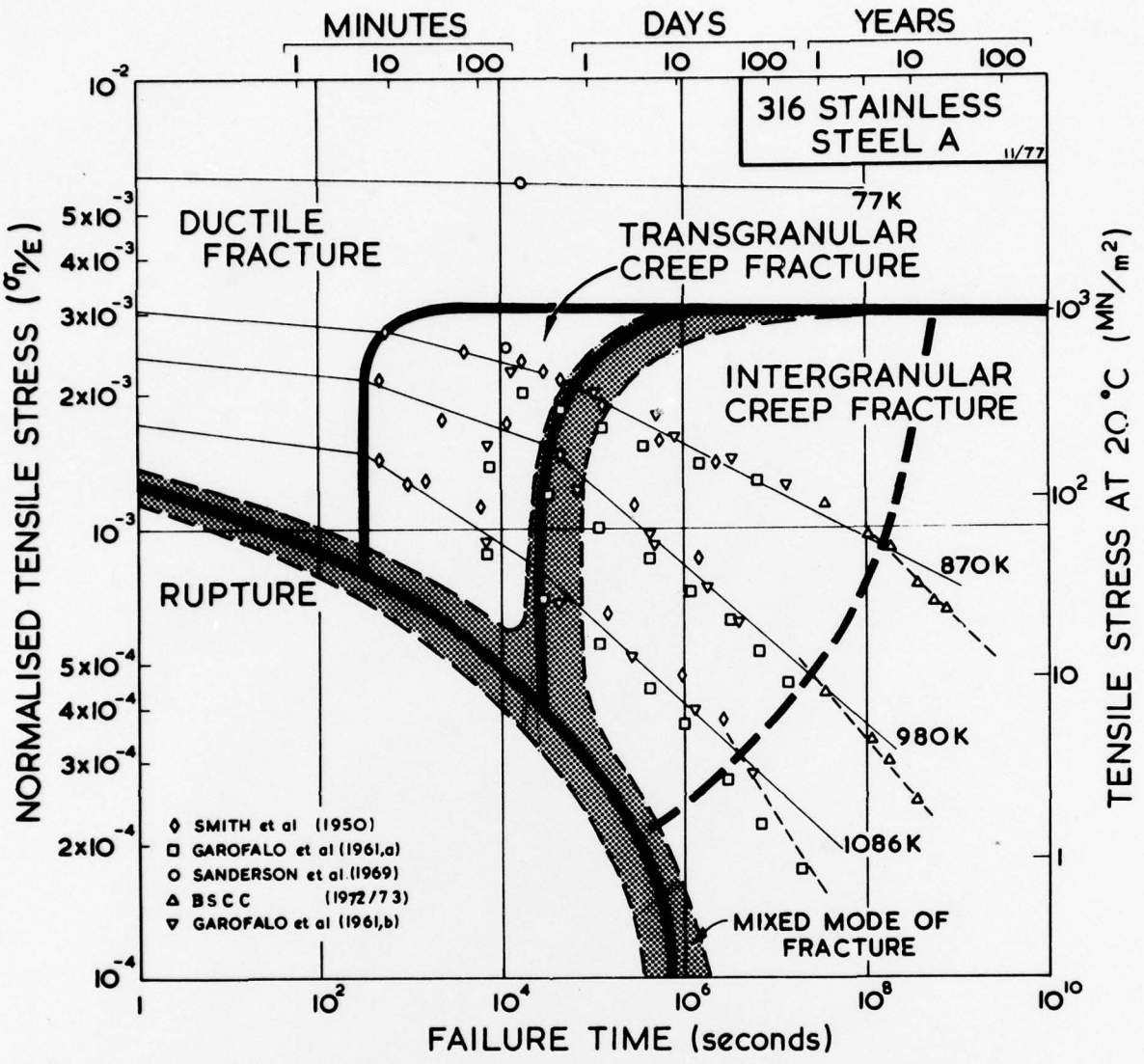

3 (b) A map of the second type for the same steel. The field boundaries have been cross-plotted from Fig. 3(a). Shading indicates a mixed, or transitional, mode of fracture.

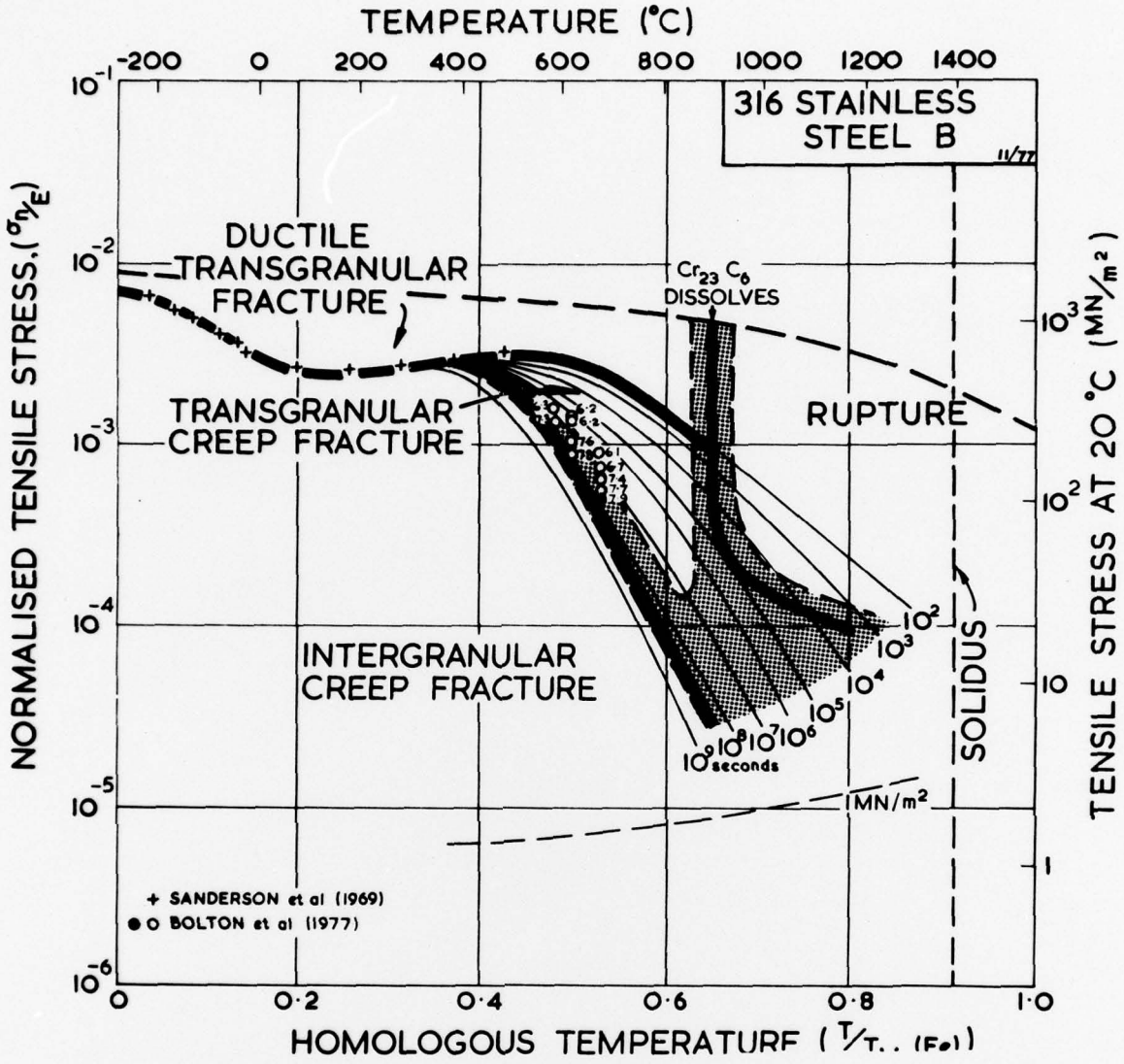

Figure 4

4 (a) A fracture map of the first type for high-boron, homogenised and air-cooled, 316 stainless steel.

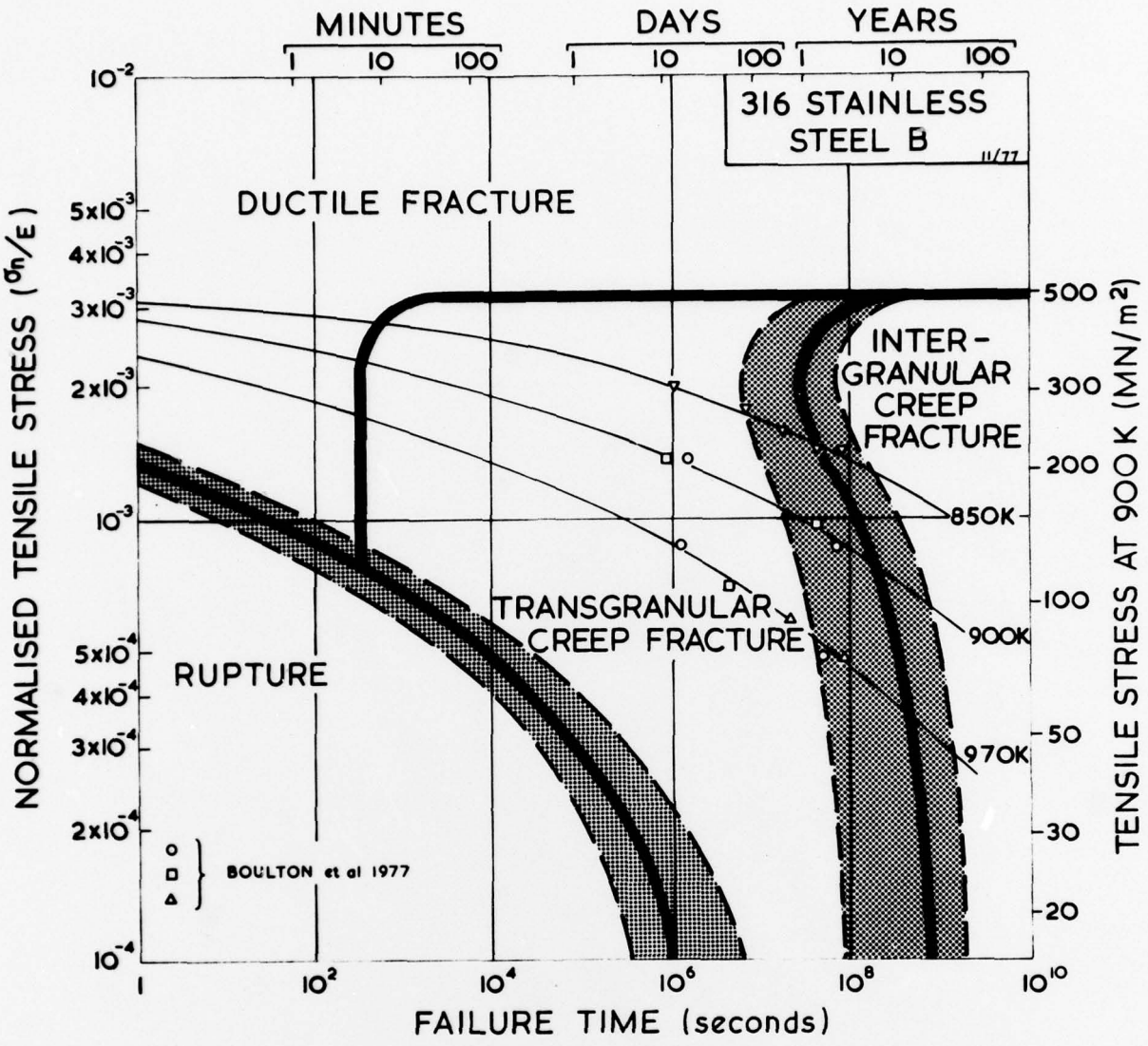

4 (b) A map of the second type for the same steel.

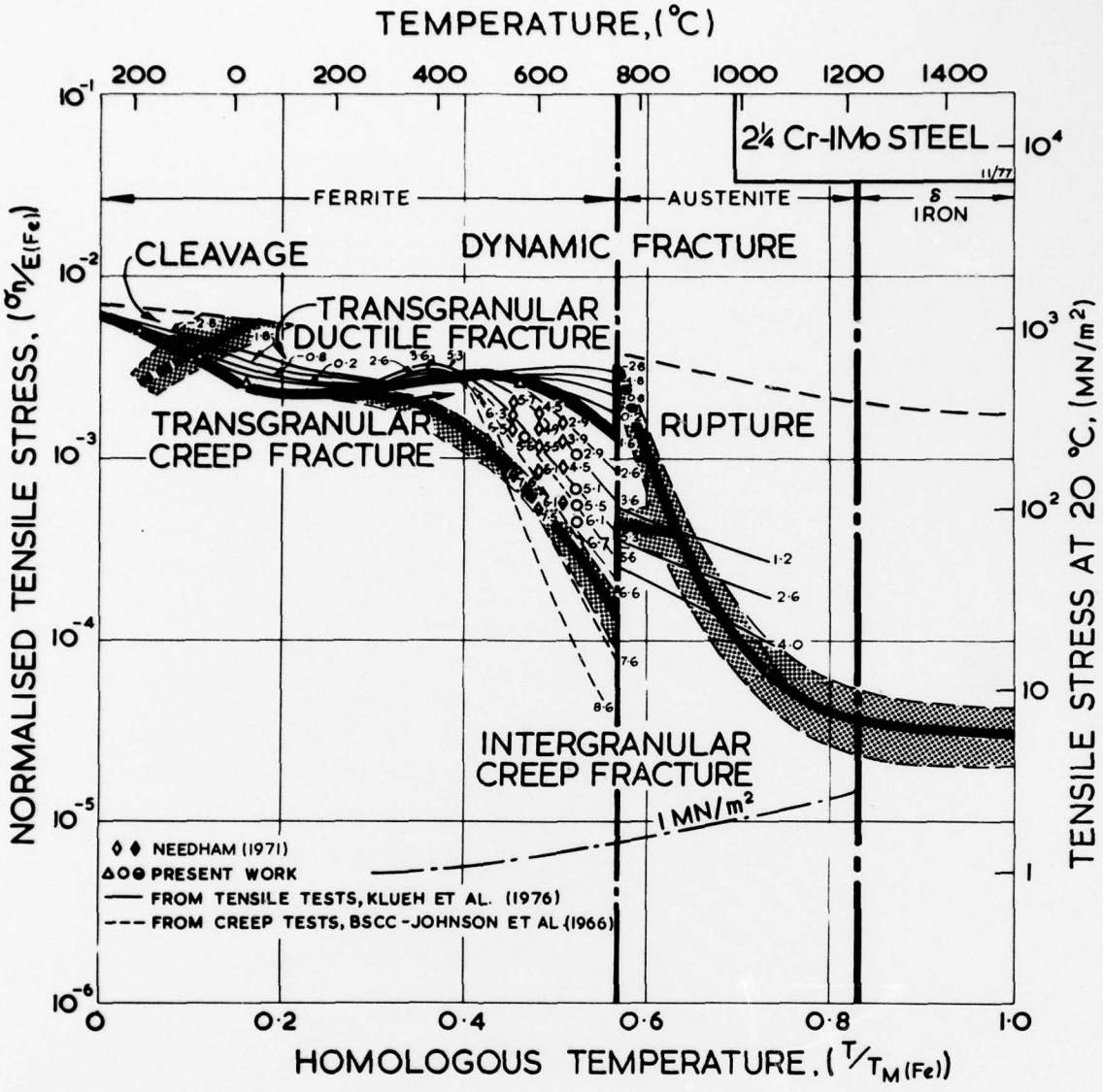

Figure 5

5 (a) A map of the first type for an annealed 2¼Cr-Mo ferritic steel.

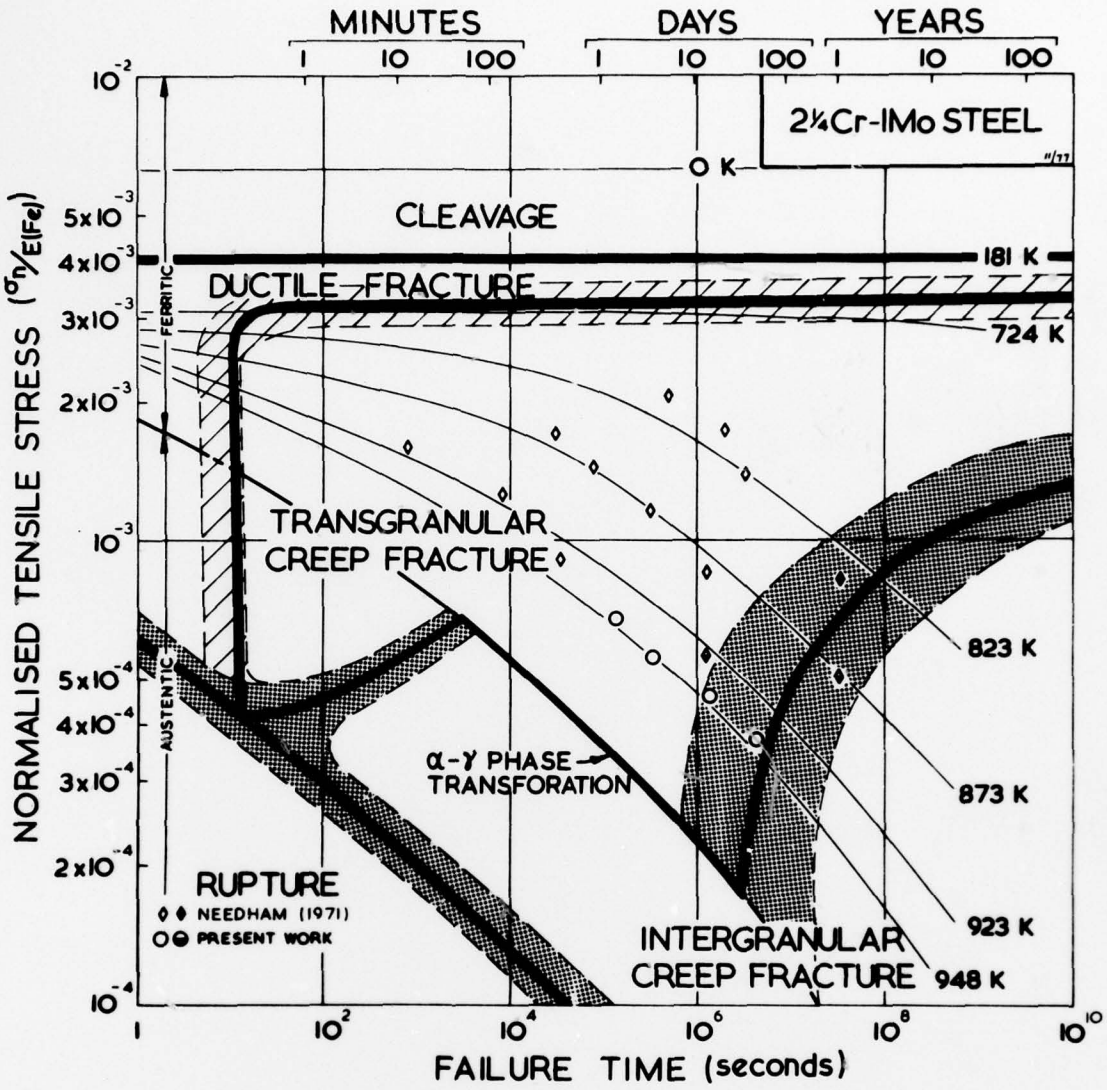

5 (b) A map of the second type for the same steel.